Polycarbonate Simulations with a Density Functional Based Force Field

P. Ballone,[†] B. Montanari,[‡] and R. O. Jones*

Institut für Festkörperforschung, Forschungszentrum Jülich, D-52425 Jülich, Germany

O. Hahn

Max-Planck-Institut für Polymerforschung, Postfach 3148, D-55021 Mainz, Germany

Received: January 22, 1999

The results of density functional calculations of the structural and vibrational properties of molecules related to polycarbonate have been used to optimize the parameters describing a classical atomistic force field. This field has then been used in extensive Monte Carlo and molecular dynamics simulations of crystalline, amorphous, and liquid polycarbonate systems. Applications include thermal properties of crystal and liquid phases, the glass transition, and vibrational properties and surface structure of the amorphous material. Molecular dynamics calculations using both this force field (DF-ff) and one derived from MD simulations of liquids (liq-ff) describe reasonably well the structure factor of amorphous bisphenol A polycarbonate.

I. Introduction

Polycarbonates are important thermoplastics, and one of the best studied is bisphenol A polycarbonate (BPA-PC). This material is characterized by good impact resistance and high glass and melting temperatures, and it has been investigated extensively over the past 40 years.[1−3] As part of a continuing study of organic molecules and polymers, we have performed density functional (DF) calculations of the structure and energy surfaces of a series of molecular analogues of BPA-PC.[4,5] These include the "immobile"[6] and "mobile"[7] crystalline forms of the closely related 4,4′-isopropylidenediphenylbis(phenylcarbonate), DPBC, the crystalline forms of the cyclic dimer and tetramer oligomers,[8] and the molecular fragments benzene, phenol, BPA, and DPBC. The smaller molecules are well studied, and the crystalline structures of the larger are known from X-ray diffraction. These systems together then have pronounced advantages as test cases over the less well characterized amorphous chains. The DF calculations of ground state geometries, vibration frequencies, and energy barriers[4,5] are in good agreement with available experimental data.[6−8]

These calculations provide a wealth of microscopic information on these systems that is otherwise difficult to obtain, but many thermodynamical and mechanical properties of interest involve time and size scales that are far beyond their reach. For these properties and systems it is customary to parameterize the forces involved, and two general approaches have been used: (a) the parameters are adjusted to reproduce accurately known experimental and theoretical data for a specific system (often with many adjustable parameters),[9] and (b) "generic" force fields are designed to describe large classes of materials reasonably well, without seeking a precise description of any. Following the pioneering work of Williams and Flory using an empirical force field,[10] there have been numerous simulations of polycarbonate systems. We now describe some of the most recent.

Amorphous cell simulations of BPA-PC have been performed by Suter and co-workers,[1,2,11] and Fan et al.[12] studied the structure factor and mechanical properties of model amorphous structures, as well as the local chain dynamics near the glass transition temperature.[13] They used the Dreiding force field,[14] modified to reproduce the results of quantum chemical calculations for the torsion barriers in diphenyl carbonate (DPC) and 2,2-diphenylpropane (DPP). Sun et al.[15] have developed a force field for polycarbonates based on Hartree−Fock calculations for carbonic acid and its phenyl and methyl derivatives,[16] scaled to reproduce experimental structural information. Molecular dynamics simulations of amorphous BPA-PC have been performed by Shih and Chen[17] using a minor modification of the Tripos 5.2 force field, which has a generic form able to describe satisfactorily many small organic molecules.[18] Whitney and Yaris[19] recently used the force field based on the united atom CHARMM potential[20] to simulate phenyl ring flips in glassy polycarbonate. We shall return below to the very recent neutron scattering measurements and simulations performed on several polycarbonate systems.[21] It can be seen that several familiar force fields have been applied to the polycarbonate family with interesting results.

In the present work we adopt a strategy between the above two: We use the extensive information available from our DF calculations of the structures, energy barriers, and dynamical properties of molecules with structures related to BPA-PC to parameterize a classical force field for use in Monte Carlo (MC) and molecular dynamics (MD) simulations. On the other hand, we facilitate these simulations by adopting a relatively simple form for the potential. The vectors defining the unit cell used in the DF calculations are taken from experiment, but no other measured data enter the parameterization of the force field, and the DF calculations themselves are free of adjustable parameters.

In section II we describe the form of the force field and the procedure used to optimize its parameters, and in section III we outline the MC and MD methods we use. In section IV we

* Corresponding author e-mail: r.jones@fz-juelich.de.

[†] On leave from Max-Planck-Institut für Festkörperforschung, Heisenbergstrasse 1, D-70569 Stuttgart, Germany. Present address: Università degli Studi di Messina, Dipartimento di Fisica, Contrada Papardo, I-98166 Messina, Italy.

[‡] Present address: Department of Physics, Queen's University, Belfast, BT7 1NN, Northern Ireland.

10.1021/jp9902598 CCC: $18.00 © 1999 American Chemical Society
Published on Web 06/19/1999

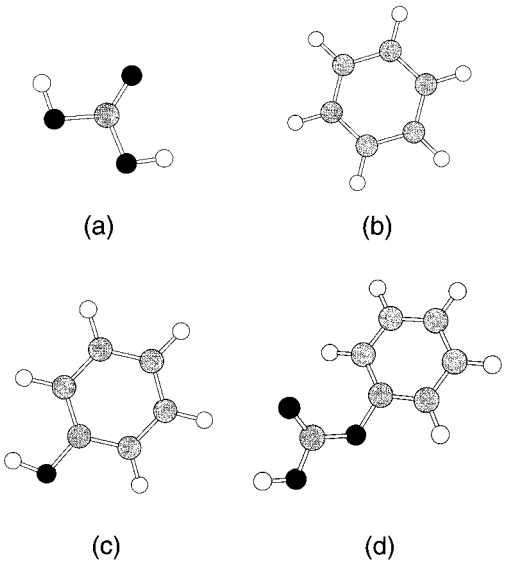

Figure 1. Molecular structures: (a) trans−trans isomer of carbonic acid; (b) benzene; (c) phenol; (d) trans−trans isomer of monophenylcarbonate.

apply the force field (referred to below as DF-ff) in MC simulations of a range of systems related to BPA-PC, including thermal properties of the crystal and liquid phases, the glass transition, vibrational properties and surface structure of amorphous DPBC, and interaction of DPBC with a single water molecule. A comparison of MD calculations with this force field and one derived from MD simulations of liquids (referred to as liq-ff) shows that some features of the calculated structure factor of amorphous BPA-PC are very similar, while others differ significantly. Our concluding remarks are presented in section V.

II. Force Field

Polycarbonates are relatively simple molecules, with covalent intramolecular bonds and intermolecular bonds of van der Waals type. The molecules that have been used to optimize the force field parameters are shown in Figures 1 and 2, and the labeling of the atoms is shown in Scheme 1. Our previous DF calculations[4] have shown that the structural parameters in these molecules are remarkably transferable, so that they are good candidates for a classical force field description. Finally, polycarbonate has one of the lowest dielectric constants ($\sim$3.0)[22,23] among plastic materials, so that a neutral atom model should be adequate. This has been utilized in several of the PC simulations mentioned above[12,17,19] and will be assumed here. The exclusion of the long range Coulomb potential terms simplifies the simulations greatly.

The functional form of our force field is similar to those used in other schemes[14,18,20,24] and includes a van der Waals term E_{vdW} and several intramolecular bonding components. E_{vdW}, which describes the short range interatomic repulsion and the long range dispersion forces that lead to intermolecular cohesion, has the Lennard−Jones (LJ) form:

$$E_{vdW} = \sum_{i,j} K_{ij}^{vdW}\left[\left(\frac{\sigma_{ij}}{r_{ij}}\right)^{12} - 2\left(\frac{\sigma_{ij}}{r_{ij}}\right)^{6}\right] \qquad (1)$$

where r_{ij} is the interatomic distance. The sum is over all pairs of atoms separated by less than $3\sigma_{ij}$, excluding those connected by chemical bonds or belonging to the same functional group (phenyl rings, carbonate and methyl groups).

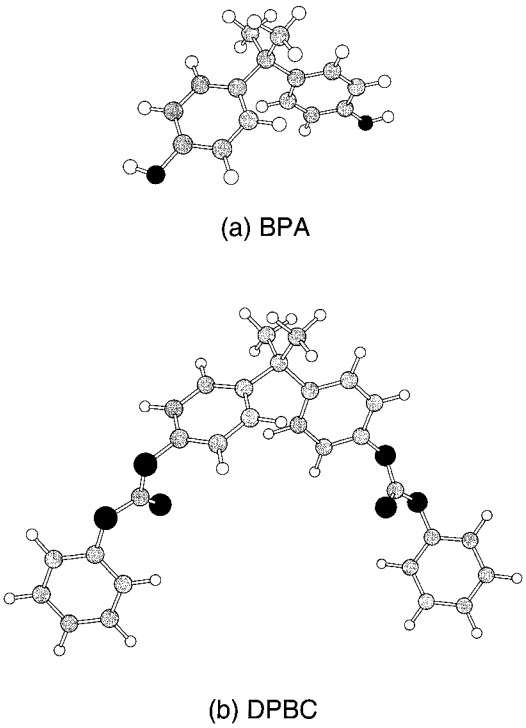

Figure 2. Molecular structures: (a) BPA, (b) DPBC.

SCHEME 1

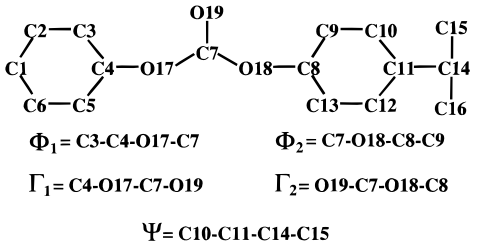

The bonding interactions include stretching (str), bending (bnd), torsional (tor), and out-of-planarity (op) contributions. The first two are

$$E_{str} = \sum_{i,j} K_{ij}^{str}[r_{ij} - r_{ij}^{0}]^2 \qquad (2)$$

$$E_{bnd} = \sum_{i,j,k} K_{ijk}^{bnd}[\theta_{ijk} - \theta_{ijk}^{0}]^2 \qquad (3)$$

where the sums include the atoms joined by covalent bonds and r_{ij}^0 and θ_{ijk}^0 are the equilibrium bond lengths and bond angles, respectively. The torsion term is

$$E_{tor} = \sum_{i,j,k,l} K_{ijkl}^{tor}[1 + \alpha \cos(\beta\, \phi_{ijkl})] \qquad (4)$$

where α is ± 1, depending on whether $\phi = 0$ describes a maximum or a minimum of the potential energy surface. The periodicity of the potential with respect to the torsion angles is determined by β, which is 3 for sp^3 angles and 2 for sp^2 angles.

The out-of-planarity term E_{op} models the energy cost of deforming the π-bond around sp^2 and aromatic carbon atoms. If we define a plane by the three nearest neighbors of such an atom, then

$$E_{op} = \sum_{i} K_i^{op}(z_\perp^2 - z_0^2) \qquad (5)$$

TABLE 1: Distances (Å) and Vibrational Frequencies (cm^{-1}) of Benzene Calculated with DF (PBE functional), the Tripos Force Field, and the DF-Based Parameterization ("new fit")

	PBE	new fit	Tripos
atoms			
C−C	1.397	1.398	1.396
C−H	1.093	1.093	1.084
mode			
C−H stretch	3127	3139	4219
C−C stretch	1588	1834	2934
C−H out-of-plane	998	1320	2187

where $z_\perp$ is the distance of the central atom from the plane and z_0 is used to reproduce the nonplanar structure of the C3−C4−C5−O17 group. This parameter is very small ($|z_0| \sim 0.02$ Å) and not essential for a good description of the BPA-PC structure. In addition, we introduce a potential term of LJ form between the terminal atoms of each quartet *ijkl* connected by chemical bonds

$$E_{1,4} = \sum_{i,j,k,l} \epsilon^*_{i,l} \left[\left(\frac{\sigma^*_{il}}{r_{il}} \right)^{12} - 2 \left(\frac{\sigma^*_{il}}{r_{il}} \right)^{6} \right] \qquad (6)$$

Our potential has obvious similarities to the standard force fields, and it is natural that we adopt one as our starting point. For the initial values we have chosen the parameters of the Tripos 5.2 force field,[18] which shares the assumption of electrostatic neutrality of the component atoms and has been used with success in an earlier simulation of amorphous BPA-PC.[17] The fitting of the potential parameters involves several steps. First, we calculate the ground state geometries and vibrational frequencies for the molecules studied in ref 4. We then focus on the structure of the mobile and immobile crystal forms of DPBC and on the energy barrier for phenyl π-fiips in the mobile crystal.[25] We have estimated this barrier by computing the total energy along the path determined in the DF computation.[4] This should be reliable, since the energy difference between the ground and transition states does not change on reoptimizing these geometries with the classical potential.

Typical results reported in Tables 1−3 show that the Tripos model describes reasonably well the structures of benzene, monophenyl carbonate, and DPBC, while the vibrational frequencies are overestimated. The same is true for phenol and BPA. The barriers for both phenyl π-flips in the condensed phases of DPBC are overestimated significantly by the Tripos field: the lowest such barrier in the "mobile" crystal form is 21.9 kcal/mol, while the DF value (7.7 kcal/mol)[4] agrees much better with experimental estimates (8−10 kcal/mol).[4]

The fit cannot be performed automatically. It is underdetermined, and any global minimization of the difference between the results of the potential and the DF values leads to unreliable values of the force constants. Nevertheless, the different degrees of freedom are largely independent, and a good fit to the DF results can be achieved with a modest effort and the following strategy. First, we refine the equilibrium bond lengths r^0_{ij} and bond angles θ^0_{ijk}, which are associated with large force constants, so that small uncertainties can lead to large errors in other degrees of freedom. Torsional angles are fixed at the original Tripos values, and we determine the force constants for stretching, bending, torsion, and out-of-planar motion by fitting the eigenvalues and eigenvectors of vibrational modes with well-defined characters: C−H, C═O, and C−O stretching, and some bending and out-of-planar modes of the carbonate group.

TABLE 2: Distances (Å), Bond and Torsional Angles (degrees), and Vibrational Frequencies (cm^{-1}) of Monophenyl Carbonate Calculated with DF (PBE functional), the Tripos Force Field, and Our DF-Based Parameterization ("new fit")

	PBE	new fit	Tripos
atoms			
C3−C4	1.393	1.399	1.402
C7−O19	1.214	1.210	1.224
C7−O17	1.359	1.375	1.334
C7−O18	1.359	1.374	1.333
O17−C4	1.413	1.414	1.395
O18−H18	0.985	0.993	0.985
H3···O19	2.562	2.54	2.55
O19−C7−O17	128.0	125.2	121.8
O19−C7−O18	125.4	124.6	121.8
C4−O17−C7	118.7	115.6	120.2
H18−O18−C7	104.5	107.3	112.2
C5−C4−O17	122.6	121.5	120.5
C3−C4 O17	115.5	117.5	118.6
C5−C4−O17−C7	47.9	46.5	48.6
mode			
O−H stretch	3531	3543	5010
C−H stretch	3153	3139	4219
C−C stretch	1591	1883	2937
C═O stretch	1772	1861	2512

TABLE 3: Distances (Å), Bond and Torsional Angles (degrees), and Vibrational Frequencies (cm^{-1}) of the DPBC Molecule Calculated with DF (PBE functional), the Tripos Force Field, and Our DF-Based Parameterization ("new fit")

	PBE	new fit	Tripos
atoms			
C3−C4	1.394	1.401	1.397
C4−O17	1.410	1.415	1.395
O17−C7	1.364	1.372	1.336
C7−O19	1.210	1.209	1.221
C10−C11	1.400	1.402	1.399
C11−C14	1.540	1.543	1.539
C14−C16	1.544	1.546	1.546
H3···O19	2.494	2.46	2.56
H9−O19	3.000	2.92	2.94
C3−C4−O17	123.2	121.1	120.7
C5−C4−O17	115.1	118.5	119.5
C4−O17−C7	119.2	116.4	117.4
O17−C7−O19	128.0	125.6	121.6
O18−C7−O19	126.9	125.0	121.2
O17−C7−O18	105.1	109.3	117.1
C9−C8−O18	121.2	120.5	120.6
C13−C8−O18	117.5	119.1	119.9
C3−C4−O17−C7 (Φ_1)	44.8	47.3	54.7
C9−C8−O18−C7 (Φ_2)	69.3	64.6	73.6
C4−O17−C7−O19	0.0	0.8	1.5
C8−O18−C7−O19	0.5	1.3	1.4
C10−C11−C14−C15 (Ψ)	8.4	4.0	4.3
mode			
C−H stretch (phenyl)	3166	3140	4219
C−H stretch (methyl)	3079	2951	4161
C−C stretch (phenyl)	1599	1908	2936
C−C stretch (methyl)	1148	1335	2002
C═O stretch	1775	1839	2501

Finally, we observe that the Lennard−Jones parameters K^{vdW}_{ij} and σ_{ij} describing the van der Waals interactions are largely insensitive to changes in the DF database, indicating that most properties of the crystalline systems should not depend strongly on their precise values. The only exceptions we have found are the equilibrium volume of the crystal phases and by the energy barrier of the phenyl π-flip, which depend sensitively on the repulsive part of the H−H and H−O intermolecular interactions.[26] Therefore, we have fixed most of the vdW

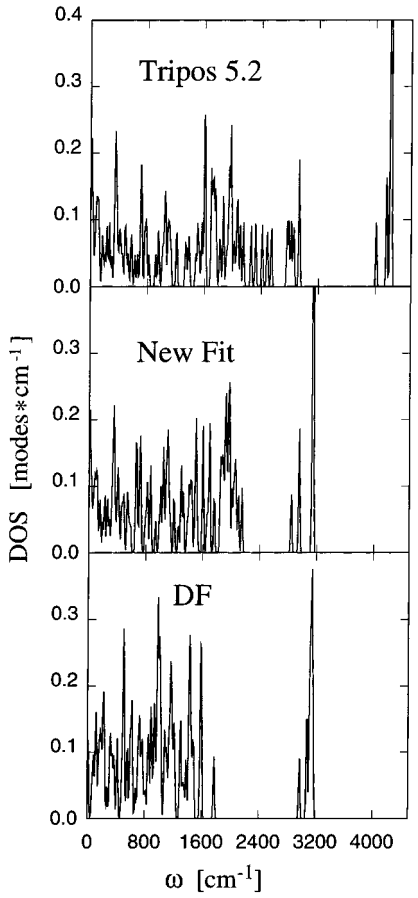

Figure 3. Total vibrational density of states of DPBC obtained with Tripos force field (top), DF calculations (bottom), and with the optimized force field (New Fit).

parameters at their Tripos 5.2 values, changing only the σ_{ij} diameters for the H−H and H−O (for the C═O group only) interactions in order to reproduce the computed phenyl π-flip barrier and the experimental equilibrium volume of the crystal phases. In the case of the O−H interaction, the usual combination rule [$\sigma_{ij} = 0.5(\sigma_{ii} + \sigma_{jj})$] is not applied. The modified force field leads to dramatic improvements, as can be seen in Tables 1−3 and Figure 3.

The DF computations of ref 4 revealed several features that are related to the quantum mechanical nature of bonding and cannot be described reliably by a simple force field. These include the difference between the C4−O17 and C7−O17 bonds, the asymmetry in the C3−C4−O17 and C5−C4−O17 bond angles, and the slight out-of-planarity of O17 in several molecules. In addition, a small part of cohesion comes from weak, unconventional hydrogen bonds between the carbonyl oxygen and the hydrogens in the phenyl rings. These details are not crucial to a description of global properties, and we have not attempted to reproduce them perfectly.

III. Monte Carlo and Molecular Dynamics Simulations

The optimized potential (DF-ff) has been used in both MD and MC simulations of polycarbonate systems. The MD results are compared with those obtained using the liq-ff force field, and we now provide details of the methods used.

A. Monte Carlo Calculations. The MC simulations were performed in the isobaric−isothermal (*NPT*) ensemble, with fixed particle number *N*, pressure *P*, and temperature *T*.[27,28] The major problem in simulating molecular phases is the presence of degrees of freedom characterized by extremely different energy scales, e.g., the stretch of covalent bonds, bending and torsion modes, and the rotation of large functional groups. The efficiency of our MC sampling has been enhanced by adopting a variety of trial displacements, including (a) single atom moves, (b) rotations of phenyl, methyl, and carbonate groups, (c) molecular rotations around the instantaneous center of mass, (d) rigid translation of molecules, and (e) homogeneous volume changes.

Single particle displacements are attempted most frequently, followed by rotations of the functional groups. Rotations and translations of the entire molecule are attempted on average every 50 single atom moves, and the volume change is attempted only every few thousand single atom moves. The relative frequency of these moves is such that individual atoms are displaced with almost equal probability in each, and the amplitude of the moves has been selected to obtain an acceptance probability of ∼0.3. We give below the lengths of MC runs in terms of single atom moves, with all other types being performed as above.

B. MD Simulation of BPA-PC Melts. Relaxation on large length scales means that the CPU time requirements of an atomistic MD are prohibitive, even for chains of moderate length.[29] This problem has been addressed by equilibrating the melts using a "coarse graining and inverse mapping" approach.[29,30] First, an atomistic polymer chain is mapped by a numerical renormalization approach onto a model ("coarse grained") chain with fewer degrees of freedom and simpler potentials than the original. MD simulations using this approach are a factor of 10^3 to 10^4 faster, allowing relaxations of a melt to be studied on large length scales. In the second step, the coarse grained melt is remapped to the underlying atomistic chains, the backbone of *each* of which is then fitted to the backbone of a coarse grained chain by adjusting the torsion angles. Finally, energy relaxation on short length scales is achieved by switching on smoothly the atomistic excluded volume interactions and performing a conventional MD simulation with the full force field.

The simulation boxes of size $L \approx 70$ Å contained 80 chains of 10 chemical repeat units, i.e., up to ∼ 30000 atoms. The coarse grained simulations were run for ≈ 15 μs. After reintroducing the atomistic structure, local relaxation was achieved by performing an atomistic MD (100−200 ps) with the YASP package.[31] The SHAKE constraints algorithm[32] was used to fix the bond lengths. This allows a longer time step (2 fs) to be used, but rules out the calculation of vibration frequencies. Static properties are not influenced by this simplification. An atomic neighbor list,[33] including all pairs within a cut-off radius of 11 Å, is updated every 15 time steps, and nonbonded interactions are evaluated within a cut-off radius of 10 Å. In section IV F, we report the comparison with the results obtained with a different potential (liq.-ff, ref 34), which includes an electrostatic term. In this case, the nonbonded interactions are evaluated within a sphere of 10 Å, with a reaction field correction for the electrostatic interactions. The effective dielectric constant was assumed to be ε_{RF} of 3.0, the static value of BPA-PC.[23]

In order to avoid a slowing down of the dynamics, the simulations have been performed at 570 K, well above the glass transition temperature (423 K).[35] *NPT* simulations at this temperature with $P = 1013$ mbar show that the experimental density (1.05 g/cm^3) is overestimated by 0.041 g/cm^3 with the DF-ff and underestimated by 0.023 g/cm^3 with the liq-ff. The isothermal compressibility, which has been determined from the volume fluctuations of smaller simulation boxes (100 mono-

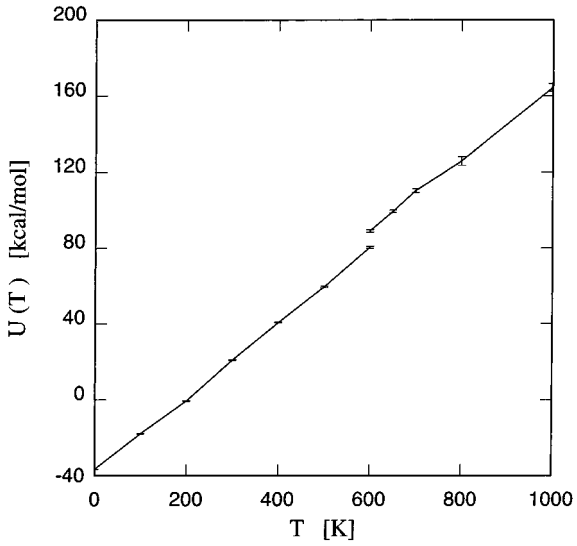

Figure 4. Temperature dependence of the average potential energy U of 72 DPBC molecules on heating the crystal. The error bars are given by the mean square fluctuation of the energy given in independent runs.

TABLE 4: Number of MC Steps Performed at Each Temperature for the Simulation of 72 DPBC Molecules (4248 atoms) and the Number of π-Flips of the Internal and External Phenyl Rings

T (K)	10^6 MC/(steps)	N_π inner ring	N_π outer ring
300	194	0	0
400	210	0	0
500	512	0	0
600	720	4	5
700	342	63	69
800	144	51	64
1000	48	51	58

mers) during 10 ns runs, yields similar values for both force fields: 0.73 and 0.62 10^{-9} Pa^{-1} for DF-ff and liq-ff, respectively. This agrees well with the observed volume shrinkage in an *NPT* simulation with $P = 5 \times 10^9$ Pa, but we know of no experimental data for the compressibility.

IV. Applications

We now present several applications of our optimized potential to simulations of molecular systems related to BPA-PC. We have noted above that the presence of X-ray diffraction data on systems related to DPBC makes them ideal test cases, and we have performed MC simulations on several. MD calculations have been performed on a model of amorphous BPA-PC.

A. Thermal Properties of Crystal and Liquid Phases of DPBC. We have performed MC simulations on a sample containing 72 DPBC molecules (4248 atoms, box size ~35 Å) at zero pressure for 300 K $\leq T \leq$ 1000 K, starting in each case from the "immobile" crystalline form, which is energetically the most stable.[36] Each sample is equilibrated during a very long sequence of MC steps (see Table 4), and average values for the potential energy U, volume V, and structural information are accumulated during the last 30×10^6 steps. The temperature dependence of the average potential energy is shown in Figure 4.

Both U and V increase smoothly with increasing T for both low and high temperatures, and there is a discontinuity at 600 K ($U(T)$ is shown in Figure 4) indicating a melting transition. The crystal structure can easily be identified at 400 K, despite the disorder present in any hot solid. The translational order is lost at 600 K, and the molecules diffuse slowly throughout the simulation cell. Large density fluctuations are observed at 1000 K (see Figure 5).

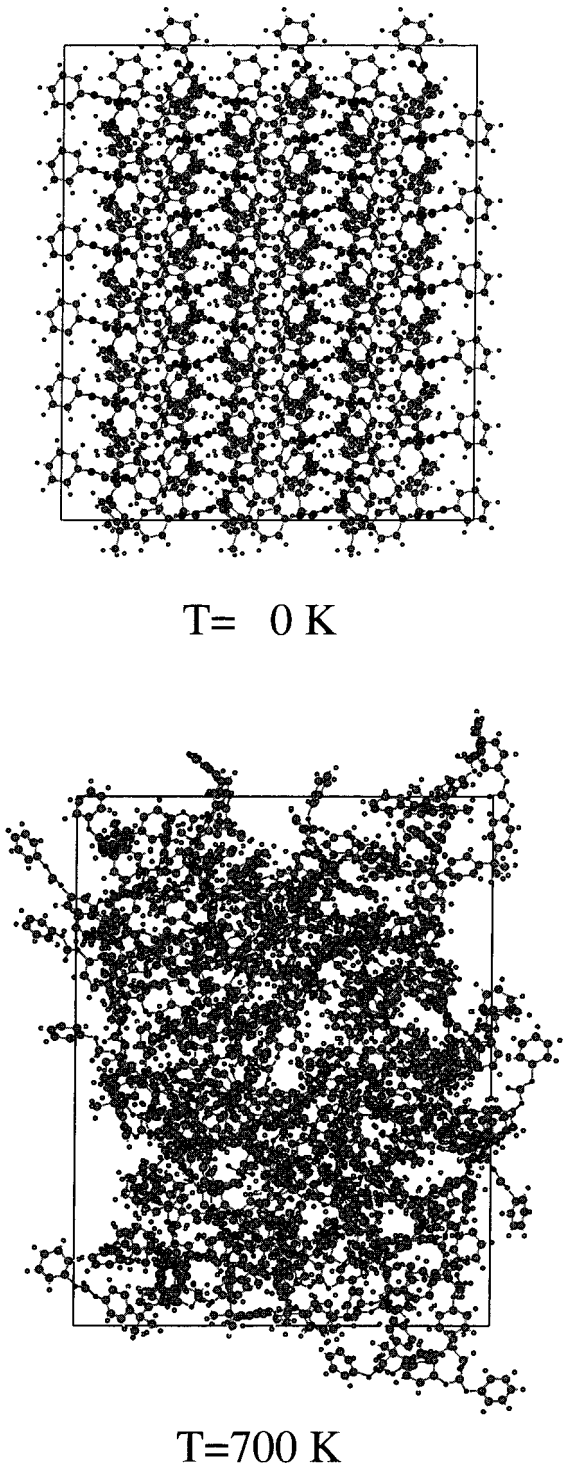

Figure 5. System studied in the MC simulation (72 DPBC molecules, 4248 atoms). We show the "immobile" crystalline structure at 0 K (top) and the equilibrated structure at 700 K.

Despite the length of the simulation,[37] the loss of translational order at 600 K provides only an upper bound to the thermodynamic melting temperature T_M, where the free energies of the solid and liquid phases are equal. This is because the (discontinuous) melting process would require a significant free energy barrier to be overcome, and this can be achieved on the simulation time scale only by overheating to the point of mechanical instability. A precise estimate of T_M would require

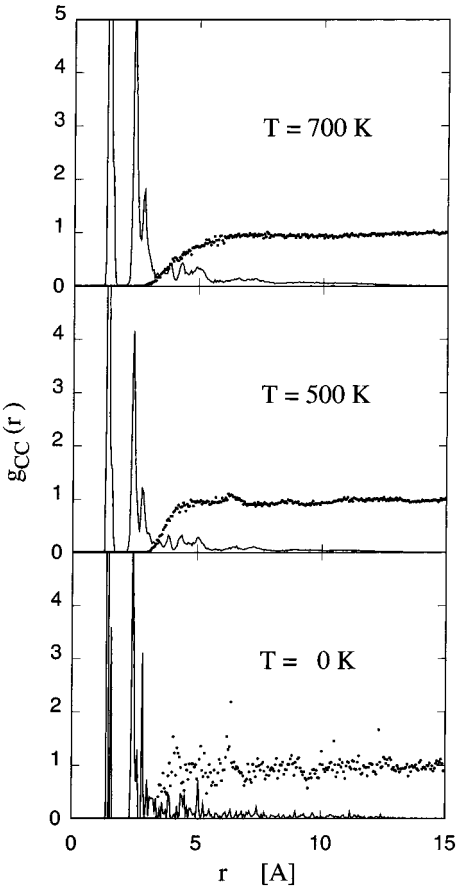

Figure 6. Radial distribution functions for C−C pairs at 0 K, 500 K, and 700 K. The solid lines represent intramolecular distances, the dots intermolecular distances.

long simulations for larger systems to determine the free energies of both phases as a function of T. These calculations have not yet been performed, but we have analyzed the structures of a series of well equilibrated systems in the crystal and liquid phases. We have focused on the temperature range (500−700 K) in which the transition is expected to occur.

The structure of a system at nonzero temperature is characterized by the radial distribution functions (RDF) $g_{\alpha,\beta}(r)$.[38] If an atom of type α is at the origin, the average number of atoms of type β at a distance r is

$$\langle dN_{\alpha,\beta}(r)\rangle_T = 4\pi r^2 \rho_\beta g_{\alpha,\beta}(r) dr \qquad (7)$$

where ρ_β is the average density of atoms β, and the brackets $\langle ... \rangle_T$ indicate a thermal average at temperature T.

In Figure 6 we show the intramolecular (full line) and intermolecular (dots) contributions to the RDF for C−C pairs for different temperatures. The corresponding curve for H−H pairs is similar. At $T = 0$ the RDF are given by a series of delta functions corresponding to the internuclear separations in the crystal. The distribution becomes denser and more continuous as r increases. The intramolecular part is short range, because of the finite size of the molecular units and the intermolecular component tends to unity as r increases, reflecting the loss of correlation in the distribution of the β component. The short range repulsion of the interatomic potentials causes the RDF to vanish at short distances.

The discrete structure of the $g_{\alpha,\beta}(r)$ disappears rapidly as T increases. Residual correlations in the hot solid at 500 K are apparent from the structure around $r = 5$ Å, while $g_{\alpha,\beta}(r)$ approaches the asymptotic value of unity in the liquid phase at 700 K. The temperature dependence of the intramolecular part of $g_{\alpha,\beta}(r)$, which is determined by the (relatively high) energy scale of the intramolecular covalent bonds and the short range repulsion, is much weaker than in the intermolecular part.

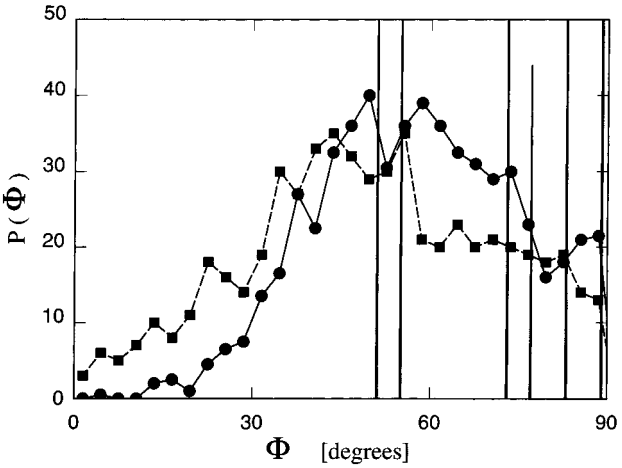

Figure 7. Distribution $P(\Phi)$ of torsional angles $\Phi_{1,2}$ at 0 K (vertical lines), 500 K (solid line, dots), and 700 K (dashed line, squares).

The distribution $P(\Phi)$ of torsional angles Φ_1 and Φ_2 (Figure 7) provides information about the orientation of the phenyl rings, which are associated with weak intramolecular restoring forces. The series of delta functions at $T = 0$ broadens rapidly as T increases. $P(\Phi)$ is independent of T above 500 K, and the small changes on melting suggest that rotational disorder may already be present in the solid. We plan to extend the present simulations to determine whether this rotational disordering is sudden (a phase transition) or a continuous change.

B. MC Simulation of the Glass Transition. The quench of liquid DPBC results in the formation of an amorphous system below a glass temperature T_g that manifests itself with a rapid increase of the viscosity coefficient η and with the (nearly) discontinuous change of the specific heat C_p and of the thermal expansion coefficient χ_T. Since our MC simulation does not provide a direct estimate of viscosity, we determine the glass temperature by analyzing the low and high temperature behaviors of C_p and χ_T.

A liquid sample of DPBC well equilibrated at 700 K is quenched progressively in runs of 3×10^6 MC steps, during each of which T is lowered discontinuously by 10 K. The entire quench takes 200×10^6 MC steps and results in a low temperature structure that is apparently disordered. Analysis of the C−C radial distribution functions confirms that the local coordination is similar to that of the liquid phase and much less structured than that of the crystal phase at the same temperature. The quench rates used here are, of course, many orders of magnitude greater than those accessible experimentally.

Although the potential energy U is a remarkably linear function of T over the entire range, a linear fit of the low (150−300 K) and high (550−700 K) temperature behaviors of $U(T)$ allows us to identify a change in the constant pressure specific heat for $T \sim 400$ K (Figure 8). We find that $C_P/(NK_B) = 3.07$ and 3.25 K^{-1} at low and high T, respectively, where N is the total number of atoms, and K_B is the Boltzmann constant. The crossing of the two linear interpolations at 410 K locates the glass point T_g of the model. The temperature dependence of the equilibrium volume (Figure 8) also shows two different linear regimes: at high T there is a large thermal expansion coefficient ($\chi_T = (\partial V/\partial T)/V = 1.8\ 10^{-3}\ K^{-1}$), and at low T the thermal expansion coefficient ($\chi_T = 5.6\ 10^{-4}\ K^{-1}$) is reduced by the gradual freezing of relaxation channels. The crossing of

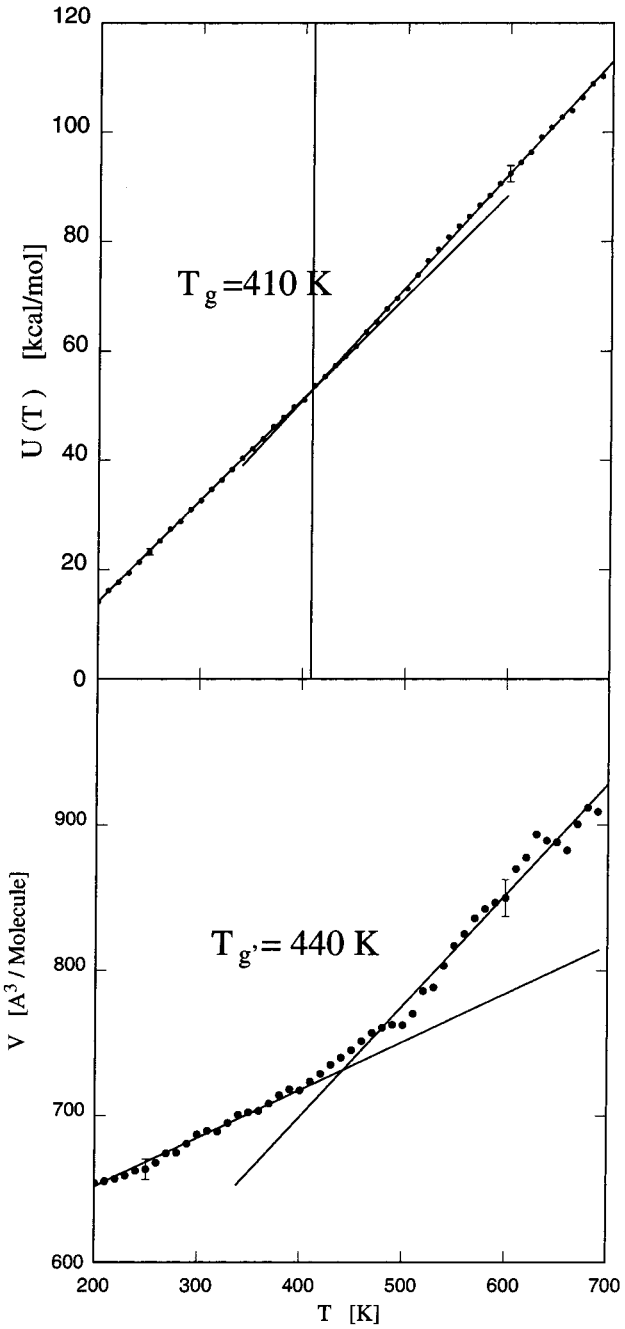

Figure 8. Plots of potential energy U (above) and volume V (below) as a function of temperature in amorphous DPBC. The intersection of the low T and high T lines gives the glass temperatures T_g and T_g', respectively. Representative error bars are reported at low ($T = 250$ K) and high ($T = 600$ K) temperatures.

the two linear parts of $V(T)$ occurs at $T_g' = 440$ K. The estimates of the glass temperature by the specific heat and by the thermal expansion coefficient bracket the experimental values of the glass temperature of BPA-PC (418−432 K).[22,25,35]

C. Vibrational Properties of Amorphous DPBC. The potential energy of the low temperature structure of amorphous DPBC has been optimized carefully as a first step towards the characterization of the vibrational properties of this model system. Since the simulated sample (72 molecules with 4248 atoms) is too large for the straightforward determination of vibrational eigenvalues and eigenvectors, we have selected subsets of M molecules (with M up to 40) as compact clusters embedded in the quenched system. The dynamical matrix of this subsystem is computed by finite differences and diagonalized by a standard routine, with the surrounding molecules simply providing the boundary condition for the computation of the potential energy of the central cluster. For all but the smallest clusters, the vibrational density of states does not depend significantly on the number of molecules in the cluster. We have performed the same computation for clusters of identical size in the immobile crystal form of DPBC for comparison purposes.

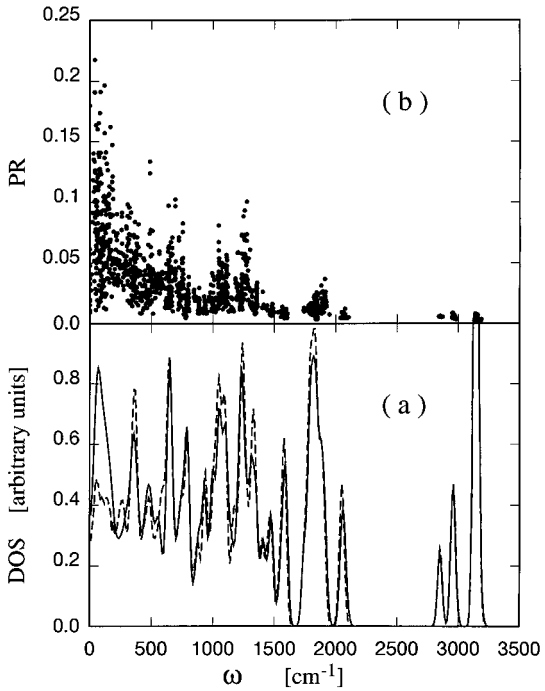

Figure 9. Vibrations of cluster containing 40 molecules: (a) vibrational density of states in the amorphous phase (full line) and the immobile crystal phase (dashed curve); (b) participation ratio $p^{\alpha}(\nu_{\alpha})$ for the vibrational modes of the amorphous cluster.

The results for the vibrational density of states of a cluster of 40 molecules (2000 atoms, diameter ~ 25 Å) are shown in Figure 9(a). As expected, the packing of the molecules affects mainly the low frequency part of the vibrational spectrum, which displays systematic differences between the crystal and the amorphous samples. In particular, we find an excess of low frequency modes in the amorphous case, in agreement with the general trend observed in a variety of ordered and disordered condensed systems.[39] Although the lowest frequency part of the vibrational spectrum is affected most by numerical uncertainties, the excess of low-frequency modes is found in all clusters we have analyzed and should be a general property of these systems. It does not depend on the particular boundary conditions used, since we always compare results for amorphous and crystal clusters of the same size and with the same boundary conditions.

The localization properties of the low frequency modes in amorphous systems is of considerable interest.[39] We have characterized this property by computing the participation ratio of each mode, defined by

$$p^{\alpha}(\nu_{\alpha}) = N\frac{[\sum_{i=1}^{N}|\mathbf{B}_i^{\alpha}(\nu_{\alpha})|^2]^2}{\sum_{i=1}^{N}|\mathbf{B}_i^{\alpha}(\nu_{\alpha})|^4} \qquad (8)$$

where α identifies the eigenmode, the index i runs over the atoms in the central cluster, and $\mathbf{B}^{\alpha}(\nu_{\alpha})$ is the eigenvector whose

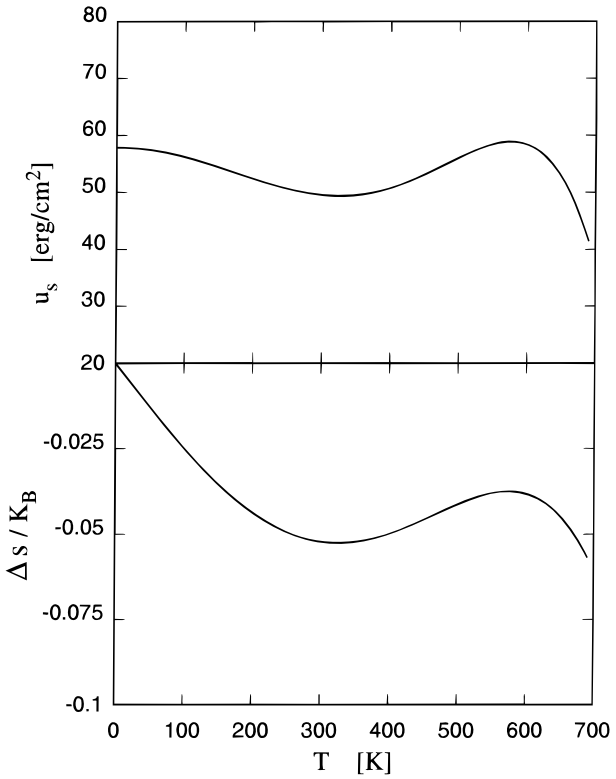

Figure 10. Temperature dependence of surface energy u_s (above) and surface entropy Δs (below).

eigenvalue is ν_α. The participation ratio approaches unity for fully delocalized modes and is $\ll 1$ for localized excitations. The values of $p(\nu)$ in the amorphous cluster with $M = 40$ are shown in Figure 9(b). We see that all the eigenstates are fairly well localized, although there is a clear trend towards increased localization at higher frequencies. The vibrational modes of the crystal sample are also well localized, and there is no clear difference between the ordered and disordered cases. This shows that the discussion of the localization properties of the vibrational modes of these systems is still outside the reach of the present simulations. On the other hand, it also explains the insensitivity of our results on the boundary conditions adopted to compute the dynamical matrix. We note that the acoustic modes, which are intrinsically delocalized, arise from intermolecular interactions only. They are therefore extremely soft and are easily localized even by small perturbations.

D. Surface Properties of Amorphous DPBC. The efficiency of the present simulations has allowed us to study the surface properties of amorphous DPBC samples, which are currently well outside the reach of DF computations. Beginning with a well-equilibrated, isotropic liquid sample of 72 DPBC molecules at 700 K, we removed the periodic boundary conditions in the *z* direction alone, creating a slab with two parallel surfaces perpendicular to the *z* axis (sample AS). This is then quenched progressively to low temperature, following a procedure analogous to the one applied in the simulation of the glass transition. The final configuration is an amorphous slab, whose central simulation cell is almost cubic with an edge of $\sim$ 40 Å. The surface energy u_s, defined as the potential energy difference between the slab and the homogeneous sample, is shown in Figure 10 as a function of temperature. Over the entire temperature range, u_s is of the order of $\sim$ 50 erg/cm^2, which is typical for polymeric materials.[40] If we follow this function during the cooling process, we observe that at high temperature $u_s(T)$ increases steadily with decreasing temperature, because

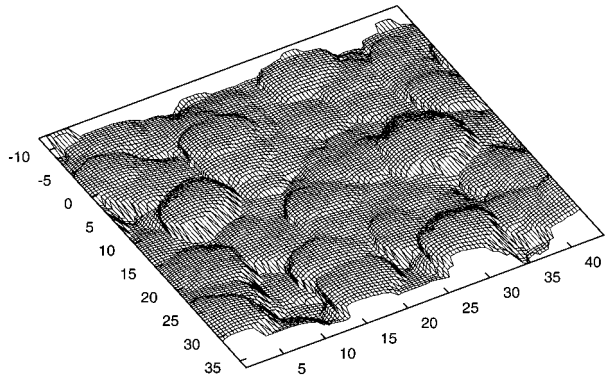

Figure 11. AFM "image" of a free surface of amorphous DPBC.

the energy cost of creating the surface increases with increasing density and cohesion in the system. This trend, however, is reversed in a wide temperature range spanning the glass temperature, in which relaxation processes appear to be more effective at the surface than in the bulk. Finally, for $T \leq 300$ K, relaxation processes are ineffective for both samples and the surface energy increases slowly with decreasing *T*. This behavior differs markedly from that observed in crystal surfaces, where the monotonic increase in u_s with increasing *T* is compensated by a rapid entropy gain at the surface.

Although the slab and the homogeneous sample are not in thermal equilibrium and standard thermodynamic relations must be applied with caution, we have used them to calculate the surface tension and the surface entropy. The latter is negative (see Figure 10),[41] and we believe that this reflects in part the greater ordering at the surface than in the bulk. The relaxation at the surface can take place at the surface at temperatures below T_g, so that the bulk dynamics is effectively frozen.

The structure has been characterized by the surface density profile $\rho_\alpha(z)$—the density of atoms of species α averaged over the *xy* plane at height *z*—and the surface topography. The former contains a thermal average for $T > 0$. Analysis of the density profile shows that the surface width, defined as the distance over which the density changes between 10% and 90% of the bulk value, is of the order of 10 Å and increases slowly with increasing *T*.

The surface topography can be probed by scanning tunneling and atomic force microscopies (STM and AFM, respectively),[42] and there has been recent progress in applying AFM to study the morphology of the surfaces of glassy polymers.[43] Here we mimic AFM by moving an additional (hydrogen) atom above the surface and determining the contours of constant potential energy or constant force on this atom. The single external atom in our simulation is an oversimplified model of the AFM tip, but more realistic atomistic models could be studied with a modest increase in computing requirements.

Figure 11 shows the contour of zero force, defined as the surface separating the attractive from the repulsive regions in the surface potential energy, measured on sample AS. This contour is accessible to AFM experiments, and the simulation shows that the surface is fairly rough, the standard deviation of the AFM surface from an interpolating plane being of the order of several Å over an area of only $\sim$2500 Å^2. Despite the roughness, the AFM topography displays clearly recognizable features, such as the elliptical protrusions corresponding to phenyl rings, which tend to be oriented parallel to the surface.

Comparison of our results with available measurements[43] shows that the length scale of our simulations is much smaller (the smallest scanning area in ref 43 is approximately 2500 Å $\times$ 2500 Å, with a linear resolution of $\sim$ 50 Å). However, future

computations could be performed with at least ten times as many atoms, while the size and resolution of the experimental images should approach those of such larger simulations. The direct comparison of experimental and computational results for the same system could improve greatly our understanding of amorphous polymeric surfaces.

E. Water in DPBC. The interaction of small molecules with polymer chains is important since chemical, optical, and mechanical properties of these materials are often affected by the presence of water, air, and/or a variety of impurities and pollutants. In the case of polycarbonates, the interaction with hot water often results in swelling and a significant reduction of desirable mechanical properties. The DF-based force field does not include atomic charges and cannot describe the details of the interactions between water molecules and polymer chains. Nevertheless, we now show that this force field can provide valuable structural information even in such systems, at least in the limit of very low water concentration.

We have used the DF-ff force field to optimize the location of a single H_2O molecule in the mobile crystal form of DPBC, whose density is comparable to that of the amorphous phase. The force field calculations allow us to study a very large number of configurations, and we find that the water molecule lies close to the carbonate group, where the structure appears to be most open. This geometry has been used as input to the DF procedure and computational parameters described in ref 4. The DF calculations, which include all charges in the system, show that there is a change in the orientation but little change in the location of the water molecule: One of the hydrogen atoms in H_2O forms a hydrogen bond with an sp^3 oxygen atom in the carbonate group, and the other appears to be attracted by the π-electrons in a nearby aromatic ring. The formation of these hydrogen bonds is reflected in the downward shift (by 80 cm^{-1}) of the highest energy stretching modes of water. Shifts of this size are well outside the uncertainties of our computation and should be readily detectable spectroscopically. We are not aware of any experimental studies of water in DPBC. NMR studies of water absorbed in precipitated polycarbonate powder have been carried out by Lee et al.[44]

This test computation shows that the DF-based force field accounts correctly for steric effects that confine the water molecule to the open space surrounding the carbonate group. To describe features such as hydrogen bonding, however, it would require at least the introduction of atomic charges. We anticipate that the location of favorable regions of configuration space by force field calculations, followed by the determination of structural details using DF calculations, will be a useful approach in other contexts.

F. Structure Factors of BPA-PC Melts. The comparison of coherent structure factors of simulated BPA-PC melts with experimental results obtained from spin-polarized neutron scattering[21] provides another test of the atomistic force field. The MD simulations have been performed with periodic boundary conditions, so that we are restricted to discrete values for the scattering vector $\underline{q}$:

$$q_x = \frac{2\pi n_x}{L} \qquad q_y = \frac{2\pi n_y}{L} \qquad q_z = \frac{2\pi n_z}{L} \tag{9}$$

The coherent structure factor is calculated from the atomistic all-atom simulation boxes according to

$$S(q) = \left(\frac{d\sigma}{d\Omega}\right)_{coh} = \sum_{ij} \langle b_i \rangle \langle b_j \rangle \exp(i\underline{q}(\vec{r}_i - \vec{r}_j)) \tag{10}$$

using the scattering lengths H: -0.3741, D: 0.6674, C: 0.6648, O: 0.5805×10^{-12} cm. In order to estimate the error in $S(q)$, all structure factors have been calculated for two simulation boxes. Errors ($\propto 1/q$) are larger for small q, which can lead to unphysical oscillations. Although in an amorphous system we can average over different directions of $\underline{q}$ to improve statistics, the system size chosen is necessary to obtain reliable results for small q.

In addition to comparing results for DF-ff with experiment, we have compared them with results from a force field (liq-ff) derived using a different procedure. In this case, the bonded interaction parameters (angle bending, torsion) have also been determined from fits to quantum chemical calculations, but we include partial charges obtained from a fit to the molecular electrostatic potential surface.[45,46] The Lennard−Jones interactions have been parameterized by means of MD simulations of liquid phenol, bisphenol-A, and diphenylene carbonate, which may be viewed as building blocks of BPA-PC. The LJ parameters were optimized to reproduce the experimental values for macroscopic quantities such as the density, enthalpy of vaporization, etc. Details of the liq-ff force field are given elsewhere.[34] Although the two force fields are constructed differently, the resulting equilibrium bond lengths, bond angles, and some torsion potentials (such as the one at the carbonate group) are in excellent agreement. Nevertheless, the LJ parameters differ considerably. The vdW radius of an aromatic carbon is 17% larger in the liq-ff, while ϵ_{LJ} is about 50% smaller. In order to study the influence of atomistic force fields on the structure factor, the *same* coarse grained melts have been taken as starting point for the atomistic simulations with the two different force fields.

Figure 12(a) shows that the structure factors of protonated BPA-PC obtained from the two force fields agree with each other and with experiment for large values of the scattering vector $q \geq 1.25$ Å^{-1}. The local order (up to $\approx$ 5Å) is described equally well by both force fields, even though the parameters of the LJ interactions are rather different, and the *average* over the individual local conformations leads to very similar $S(q)$. For $q \leq 1.25$ Å^{-1} the force fields yield similar structure factors but deviate systematically from the experimental results. These observations also hold qualitatively for the structure factors of "methyl-deuterated" BPA-PC (Figure 12(b)), where the hydrogens of the methyl groups are replaced by deuterium.

The discrepancy at small q may originate in the atomistic force fields, the coarse grained force field, or both: The monomeric building block of BPA-PC (from carbonate-C to carbonate-C) is intrinsically stiff, and atoms belonging to the same chain show pronounced correlations over the range of a chemical repeat unit (12 Å). These correlations depend on the torsion angles between successive carbonate groups, and hence on the atomistic potentials. The bond angle potentials in the coarse grained simulations mediate forces on the same length scale. Because of chain connectivity, these forces lead to polymer-specific correlations of atom groups that are sustained up to distances of the order of the persistence length of BPA-PC.

Tschöp et al.[29] showed that the mean squared end-to-end distance, as well as the ratio of cis−trans to trans−trans conformations at the carbonate group obtained from the coarse grained simulations is in very good agreement with experiment, which gives good confidence in the coarse graining approach. On the other hand, the crucial role played by the force field in determining the structure factor, even for small q, is evident in Figure 13, where we show three stages of the relaxation process in a BPA-PC melt. The first curve corresponds to the structure

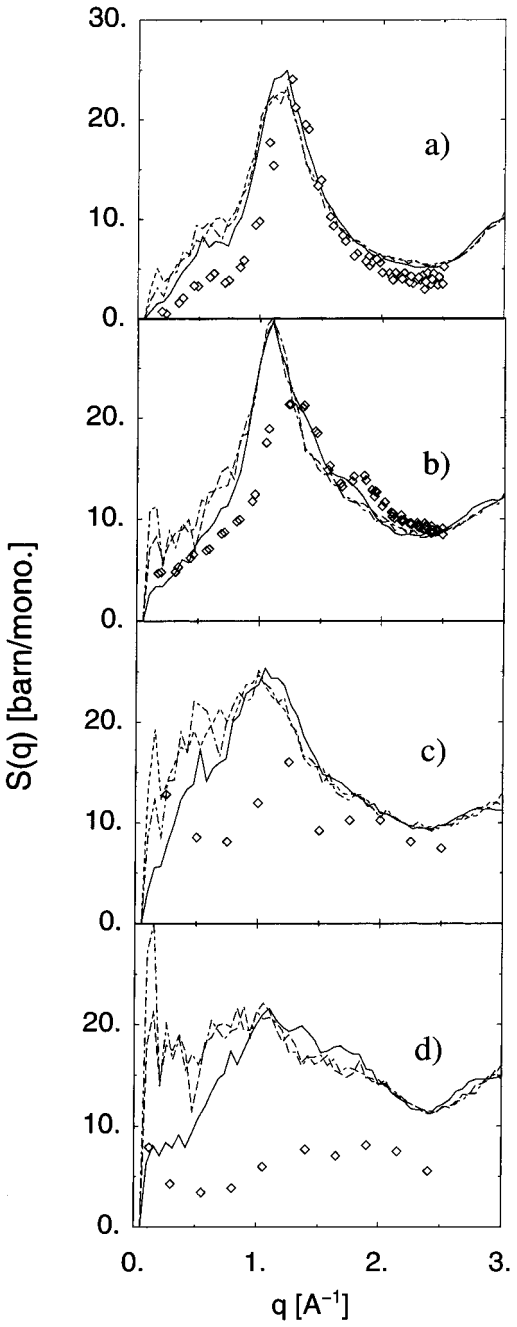

Figure 12. Structure factors of BPA-PC melts: (a) protonated; (b) methyl groups deuterated; (c) phenyl groups deuterated; (d) fully deuterated. Results from two different MD simulation boxes using DF-ff (dot-dashed: box A, dashed: box B) are compared with experiment (diamonds, ref 21) and with simulations using liq-ff (full curve, average of four boxes).

factor after the geometry optimization but before the melt is exposed to details of the atomistic force field in the MD.[47] The second and third curves show the structure factor after 10 ps and 200 ps of the subsequent atomistic MD run with the liq-ff. The change of the structure factor after switching on the atomistic potentials demonstrates their importance for the structure factor, even at small q. On the other hand, the atomistic relaxation appears to occur within a few picoseconds, and there is no trace of any long-lasting relaxation process that would change the curve shape for times accessible with atomistic MD. The same applies for the DF-ff. Electrostatics play little role in determining the statics of BPA-PC melts: If the charges are switched off in simulations with the liq-ff, the structure factors

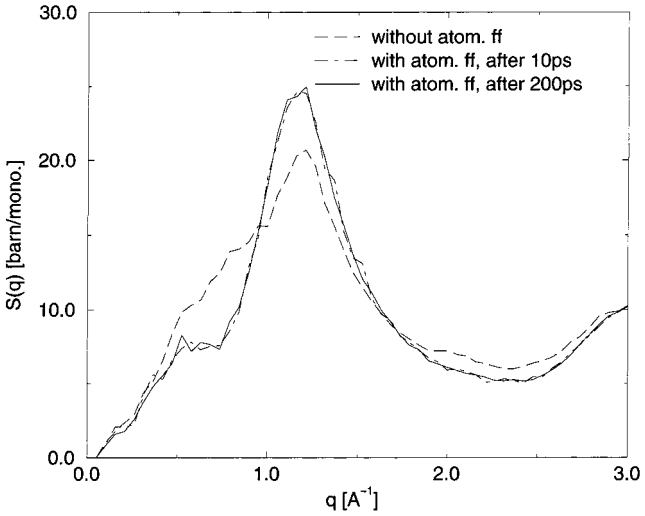

Figure 13. Structure factor of BPA-PC melt during inverse mapping procedure. Dashed, after remapping (before atomistic MD); dot-dashed, after 10 ps atomistic MD; full curve, after 200 ps atomistic MD.

are not significantly different (statistically) from those obtained with the "full" liq-ff.

Tschöp et al.[30] also performed structure factor calculations employing atomistic simulations with the AMBER force field.[24] Their results agree much better with experiment than those obtained with both force fields used here, and it is possible that more complicated atomistic force fields with many cross terms for the bonded interactions (e.g., refs 9, 15) may be needed in general to provide better agreement with experiment. Such force fields are, of course, much less suited to MD simulations.

A study of the parameters of the DF-ff and liq-ff force fields sheds light on the similarity of the structure factors they give. The torsion angles along the backbone of a polymer chain are crucial in determining its conformation, and those at the carbonate group (Φ_1 and Φ_2) are decisive, since the torsion barrier (C10−C11−C14−C15) at the phenyl ring is very small in both force fields. The other torsion at the phenyl group (C7−O18−C8−C9) determines the rotation state of the phenyl ring with respect to the carbonate group. This barrier differs in the two force fields and could contribute to the differences between their results at small q. In fact, the largest deviations between simulation and experiment occur for the structure factors involving deuterated phenyl rings, and they are most pronounced for fully deuterated BPA-PC (Figure 12(c,d)). Indeed, intrachain correlations over $\sim$ 12 Å found in structure factors of TMC-PC[21] indicate that the bonded interactions are very important in the polycarbonate family.

There are sources of error unrelated to the force fields. The neutron scattering experiments have been performed at temperatures near 0 K, in contrast to the simulation temperature of 570 K. Quenching the system to 0 K in a 30 ps run showed no significant improvements, although this quenching rate is orders of magnitude faster than those accessible experimentally. Finally, the preparation of the sample included a pressing, which could also change the experimental structure factors.

V. Conclusions

The results of density functional calculations of the structures, energy barriers, and vibration frequencies of polycarbonate and related molecules have been used as a database for determining the parameters of a force field for use in classical simulations. The force field has a standard form, and the optimized form is

able to reproduce much of the detail of the DF energy surfaces. We have used it to carry out classical simulations for polycarbonate systems with length and time scales far beyond those accessible to density functional studies.

Extensive Monte Carlo calculations have been performed on a range of systems, with particular focus on 4,4′-isopropylidenediphenylbis(phenylcarbonate) (DPBC), a molecule closely related to polycarbonate. This molecule crystallizes in two forms ("mobile", "immobile"), whose structures are known with precision, and we have studied the thermal properties of the crystal and liquid phases as well as the glass transition. Our estimate of the glass transition temperature (410−440 K) agrees satisfactorily with experimental estimates (418−432 K). The vibrational spectrum calculated for a cluster of 40 DPBC molecules embedded in the quenched system shows an excess of low-frequency modes in the amorphous system. The first results of model calculations of atomic force microscopy of amorphous DPBC surfaces indicate that such simulations should provide valuable information about the structure of amorphous surfaces.

Two other types of calculation have been performed: We have used the force field to find the favored location of an isolated water molecule in the mobile crystalline form of DPBC, and we have refined the structure found using DF calculations. These calculations indicate that the location of favorable regions of the energy surface using force field calculations, followed by structural refinement using DF calculations, provide a promising combination for investigating polycarbonate and related materials. Finally, we have performed extensive molecular dynamics calculations of the structure factor of amorphous BPA-PC using both the DF-based force field (DF-ff) and one derived from MD simulations of liquids (liq-ff). Although neither force field describes the relative disposition of the phenyl rings accurately, both give a satisfactory description of the structure factor in BPA-PC. We have discussed the differences between the two force fields in detail.

It is encouraging that a force field based on DF-energy surfaces, and free of empirical data, can provide useful results in the case of BPA-PC, as the method can also be applied in other systems for which experimental data are unavailable or difficult to obtain.

Acknowledgment. The MC and MD simulations were performed on DEC AXP servers and work stations in Jülich and Mainz, and the work was supported in both places by the MaTech Program (03N8008) of the Bundesminister für Bildung, Wissenschaft, Forschung und Technologie, Bonn. We thank other participants in this project, particularly K. Kremer and F. Müller-Plathe (MPI für Polymerforschung, Mainz), for numerous discussions and suggestions, and K. Kremer for a critical reading of the manuscript. The DF calculations were performed on the Cray T3E-600/512 and T3E-900/256 computers in the Forschungszentrum Jülich with grants of CPU time from the Forschungszentrum and the John von Neumann-Institut für Computing (NIC).

Supporting Information Available: The parameters in the DF-based force field that differ from those of the Tripos 5.2 force field are available as Supporting Information. This material is available free of charge via the Internet at http://pubs.acs.org.

References and Notes

(1) Hutnik, M.; Argon, A. S.; Suter, U. W. *Macromolecules* **1991**, *24*, 5970, and references therein.

(2) Tomaselli, M.; Robyr, P.; Meier, B. H.; Grob-Pisano, C.; Ernst, R. R.; Suter, U. W. *Macromolecules* **1996**, *89*, 1663.

(3) See, for example, Goetz, J. M.; Wu, J.; Yee, A. F.; Schaefer, J. *Macromolecules* **1998**, *31*, 3016, and references therein.

(4) Montanari, B.; Ballone, P.; Jones, R. O. *Macromolecules* **1998**, *31*, 7784.

(5) Montanari, B.; Ballone, P.; Jones, R. O. *Macromolecules* **1999**, *32*, 3396.

(6) Perez, S.; Scaringe, R. P. *Macromolecules* **1987**, *20*, 68.

(7) Henrichs, P. M.; Luss, H. R. *Macromolecules* **1988**, *21*, 860.

(8) Brunelle, D. J.; Garbauskas, M. F. *Macromolecules* **1993**, *26*, 2724.

(9) A recent example is the quantum mechanical force field (QMFF) derived for amides, peptides, and related compounds. See Maple, J. R.; Hwang, M.-J.; Jalkanen, K. J.; Stockfisch, T. P.; Hagler, A. T. *J. Comput. Chem.* **1998**, *19*, 430 and references therein. This force field contains 732 force constants and reference values.

(10) Williams, A. D.; Flory, P. J. *J. Polym. Sci., Polym. Phys. Ed.* **1968**, *6*, 1945.

(11) Theodorou, D. N.; Suter, U. W. *Macromolecules* **1985**, *18*, 1467.

(12) Fan, C. F.; Çagin, T.; Chen, Z. M.; Smith, K. A. *Macromolecules* **1994**, *27*, 2383.

(13) Fan, C. F.; Çagin, T.; Shi, W.; Smith, K. A. *Macromol. Theory Simul.* **1997**, *6*, 83.

(14) Mayo, S. L.; Olafson, B. D.; Goddard, W. A., III *J. Phys. Chem.* **1990**, *94*, 8897.

(15) Sun, H.; Mumby, S. J.; Maple, J. R.; Hagler, A. T. *J. Am. Chem. Soc.* **1994**, *116*, 2978.

(16) Sun, H.; Mumby, S. J.; Maple, J. R.; Hagler, A. T. *J. Phys. Chem.* **1995**, *99*, 5873.

(17) Shih, J. H.; Chen, C. L. *Macromolecules* **1995**, *28*, 4509.

(18) Clark, M.; Cramer, R. D., III; Van Opdenbosch, N. *J. Comput. Chem.* **1989**, *10*, 982.

(19) Whitney, D. R.; Yaris, R. *Macromolecules* **1997**, *30*, 1741.

(20) Nilsson, L.; Karplus, M. *J. Comput.Chem.* **1986**, *7*, 591.

(21) Eilhard, J.; Zirkel, A.; Tschöp, W.; Hahn, O.; Kremer, K.; Schärpf, O.; Richter, D.; Buchenau, U. *J. Chem. Phys.* **1999**, *110*, 1819.

(22) Brydson, J. A. *Plastics Materials;* Butterworth: London, 1982; p 511, gives a static dielectric constant of 3.17 and a glass temperature of ∼ 418 K.

(23) Measurements carried out at Bayer AG, Leverkusen, Germany, Department ZF-TVG5 give a value of 3.0 (private communication).

(24) Weiner, S. J.; Kollman, P. A.; Nguyen, D. T.; Case, D. A. *J. Comput. Chem.* **1986**, *7*, 230.

(25) Henrichs, P. M.; Luss, R. H.; Scaringe, R. P. *Macromolecules* **1989**, *22*, 2731. These authors give a glass temperature of 432 K, but it is not clear whether this refers to the molecular or polymeric system. In general, the glass temperature for polymers is higher than for monomeric systems.

(26) The cohesive energy will also depend on the van der Waals parameters, but it is not well known either from DFT computations or experimental measurements and cannot be used to optimize the vdW parameters.

(27) Andersen, H. C. *J. Chem. Phys.* **1980**, *72*, 2384.

(28) Parrinello, M.; Rahman, A. *Phys. Rev. Lett.* **1980**, *45*, 1196.

(29) Tschöp, W.; Kremer, K.; Batoulis, J.; Bürger, T.; Hahn, O. *Acta Polym.* **1998**, *49*, 61.

(30) Tschöp, W.; Kremer, K.; Hahn, O.; Batoulis, J.; Bürger, T. *Acta Polym.* **1998**, *49*, 75.

(31) Müller-Plathe, F. *Comput. Phys. Commun.* **1993**, *78*, 77.

(32) Ryckaert, J. P.; Ciccotti, G.; Berendsen, H. J. C. *J. Comput. Phys.* **1977**, *23*, 327.

(33) Allen, M. P.; Tildesley, D. J. *Computer Simulation of Liquids;* Clarendon Press: Oxford, 1987.

(34) Mooney, D. A.; Hahn, O.; Müller-Plathe, F.; Kremer, K. *Comput. Theor. Polym. Sci.,* submitted.

(35) Sommer, K.; Batoulis, J.; Binder, K.; Gentile, F. T.; Heermann, D. W.; Jilge, W.; Kremer, K.; Laso, M.; Ludovice, P. J.; Morbitzer, L.; Paul, W.; Pittel, B.; Plaetschke, R.; Rueter, R.; Suter, U. W.; Timmermann, R.; Weymans, G. *Adv. Mater.* **1991**, *3*, 590.

(36) The use of temperatures at which the real system is chemically unstable is simply a strategy to equilibrate rapidly the system in the liquid phase.

(37) The length of the MC runs is of the order of 10^9 single atom moves in the temperature interval 500 K $\leq T \leq$ 700 K.

(38) Hansen, J. P.; McDonald, I. R. *Theory of simple liquids,* 2nd ed.; Academic: London, 1986.

(39) See, for example, Anderson, P. W.; Halperin, B. I.; Varma, C. M. *Philos. Mag.* **1972**, *25*, 1. Yonezawa, F. *Solid State Phys.* **1991**, *45*, 179.

(40) Dee, G. T.; Sauer, B. B. *Adv. Phys.* **1998**, *47*, 161.

(41) The surface entropy is the difference between the entropies of the system *with* and *without* a surface, and it is not positive definite.

(42) See, for example: Lüth, H. *Surfaces and interfaces of solids*, 2nd ed.; Springer: Berlin, Heidelberg, 1993. Sarid, D. *Scanning force microscopy;* Oxford University Press: Oxford, 1991.

(43) See, for example, Kowalewski, T.; Schaefer, J. *PMSE Preprints* **1997**, *76*, 215 and to be published.

(44) Lee, P. L.; Xiao, C.; Wu, J.; Yee, A. F.; Schaefer, J. *Macromolecules* **1995**, *28*, 6477.

(45) Singh, U. C.; Kollman, P. A. *J. Comput. Chem.* **1984**, *5*, 129.

(46) Besler, B. H.; Merz, K. M., Jr.; Kollman, P. A. *J. Comput. Chem.* **1990**, *11*, 431.

(47) Some gross characteristics of the atomistic force field are incorporated in the coarse grained potentials and thus in the coarse grained melt.